RSC Advances

PAPER

View Article Online
View Journal | View Issue

Cite this: *RSC Adv.*, 2026, **16**, 7550

IR and Raman spectroscopy reveal amino acid–surface interactions on B- and N-doped hydroxylated graphene quantum dots: a DFT study

Berke Özgür Arslan and Mine Yurtsever *

Graphene quantum dots (GQDs), available in a variety of sizes and morphologies, have emerged as versatile nanomaterials with broad applicability across numerous fields, particularly in biomedicine. Most experimental and theoretical studies have focused on either dopant effects or surface functionalization independently, often using relatively large graphene models. A molecular-level understanding of how B/N doping and hydroxyl functionalization jointly influence biomolecular adsorption and spectroscopic signatures at the ultrasmall GQD scale remains limited, motivating the present DFT investigation of amino acid–GQD interactions. In this study, we investigate the physisorption behavior of individual amino acid molecules on pristine and hydroxyl-functionalized GQDs, as well as on their B/N doped counterparts, to gain insights into potential interactions relevant to protein environments. All calculations were performed using density functional theory (DFT) at the M06-2X/6-31G(d,p) level. Pristine GQDs with a lateral dimension of 1.3 nm, together with their singly/doubly doped and hydroxyl-functionalized variants, were fully optimized. Electronic properties and vibrational signatures were obtained through IR and Raman spectral analyses. Glycine (Gly) and serine (Ser) were subsequently adsorbed onto the modified GQD surfaces to quantify adsorption energies and assess changes in their electronic and spectroscopic properties. For hydroxyl-functionalized GQDs, the most stable adsorption configurations involved the formation of dual hydrogen bonds between the functional groups and the amino acids. The relative positioning of dopant atoms significantly influenced the stabilization or disruption of π-electron density across the GQD surface. These structural modifications produced notable enhancements in electronic properties, including band-gap modulation and increased affinity for noncovalent interactions. Overall, both functionalization and doping substantially improved amino acid adsorption, regardless of amino acid type.

Received 5th January 2026
Accepted 29th January 2026

DOI: 10.1039/d6ra00110f

rsc.li/rsc-advances

1 Introduction

Graphene is a "two-dimensional" sp^2-hybridized carbon sheet with a honeycomb lattice structure. In contrast to other 2-D structures such as graphyne (which contains both sp- and sp^2-hybridized C atoms) or BN sheets, it has a smaller band gap, resulting in excellent electronic properties. These properties arise from extended π-electron delocalization over a virtually infinite surface, giving rise to a zero band gap. It has found numerous applications in electronics, including ultra-high-frequency transistors, light-emitting devices, touch screens, photodetectors, ultrafast lasers, and solar cells.[1] Recently, graphene has been studied for its potential as a drug carrier.[2–5] Although pristine graphene possesses many remarkable properties, such as its inertness, absence of a band gap, and low solubility, these can limit some applications. Graphene is thus modified through functionalization (the addition of functional groups) or heteroatom doping. Heteroatom doping and surface functionalization are well-established strategies to tailor the electronic and optical properties of GQDs for biosensing and bioanalytical applications. Heteroatom dopants such as B and N can modulate charge density and surface functionality, thereby altering adsorption behavior and spectroscopic signatures, forming the basis for improved biological detection.[6–8]

Functionalization can occur either covalently or non-covalently. In the noncovalent mode, π-delocalization of graphene remains intact, while in the covalent mode, graphene is bonded covalently to different organic compounds to enhance hydrophilicity and solubility in common organic solvents.[9–13]

It was observed that the electronic properties of graphene are altered upon adsorption, which led to its use as a chemical sensor.[14,15] However, pristine graphene was not found to be selective for various chemicals; therefore, doping was proposed. Doping introduces a 3-D structure into graphene sheets. Common elements with which graphene may be doped include B, N, Al, Ag, Cu, Au, Pt, and Ti.[16] Al-doped graphene can detect acetyl halide molecules, while certain ether molecules enhance the adsorption of halomethane gases from physisorption into the chemisorption region, thereby imparting selectivity.[17] Ti

Istanbul Technical University, Dept. of Chem.34469, Istanbul, Maslak, Turkey. E-mail: mine@itu.edu.tr

doping has been shown to confer selectivity in the adsorption of harmful gases on graphene, such as SO_2, NO, HCHO, and CO.[18] Functionalization is another method for altering the optoelectronic properties of graphene. Functionalized graphene is proposed as a biosensor: aminated graphene can function as a biologically active field-effect transistor for DNA detection.[19] Graphene derivatives are potent drug carriers due to their ability to release adsorbed drugs selectively.[20] They are proposed as pH-, temperature-, and photosensitive drug carriers. For example, AlN- and AlP-doped graphene were theoretically proposed as carriers for the drug 5-fluorouracil. Theoretical studies have also examined their use in detecting betalapachone, acetone, doxorubicin, and camptothecin.[21]

The adsorption properties of amino acids (AAs) on pristine, doped, and functionalized graphene surfaces have been extensively studied in recent years. Research focused on AA adsorption on graphene oxide. Considering zwitterionic and neutral Gly interactions separately, it was found that non-dissociative modes of interaction were more exothermic than dissociative modes [22]. The transport properties of graphene during the adsorption of histidine were evaluated, highlighting the existence of NH_2 and COOH groups in histidine compared to their absence.[23] Results indicated strong physisorption of histidine, whereas this was not observed in imidazole, which lacks NH_2 and COOH groups. Investigations into the interactions between Ala, Arg, Asn, Cys, and His AAs with graphene and BN nanosheets demonstrated that BN nanosheets provide a superior surface for AA adsorption than graphene.[23] Saha and Bhattacharyya conducted a thorough study on the impact of doping on functionalized graphenes with electron-deficient B and electron-excess N atoms using DFT.[24] They analyzed the adsorption of four AAs—Ala, Ser, Phe, and Tyr—on a graphene surface functionalized with –OH, $–NH_2$, and –COOH groups. When graphene is functionalized with –OH, $–NH_2$, and –COOH groups, the carbon atom at the functionalized site becomes sp^3 hybridized, the adsorption site assumes a 3-D structure, and aromaticity is disrupted. Generally, a decrease in adsorption energy upon N doping was observed, with the most energetically favorable complexes being functionalized by COOH due to the formation of double hydrogen bonds between the functionalized surface and the amino acids. Additional valuable studies in the literature include amino acid adsorption on B/N doped graphene,[24,25] biomolecule adsorption,[26–29] interactions of nucleobases and aromatic amino acids with graphene oxide and graphene flakes,[30] adsorption characteristics of amino acids on graphene and germanene,[31] and interactions of aromatic AAs with graphene and CNTs.[32]

In this work, we present a systematic and integrated DFT investigation of amino acid adsorption on ultrasmall ($\approx$1–2 nm) GQDs, incorporating both B/N heteroatom doping and hydroxyl surface functionalization. Unlike prior studies that typically address dopant effects, surface functionalization, or biomolecular adsorption separately, this study reveals how dopant identity, dopant proximity, and OH groups collectively govern charge redistribution, vibrational (IR and Raman) signatures, and adsorption behavior at the quantum-confined GQD scale. By directly correlating structural motifs with spectroscopic responses, the work provides molecular-level insight into structure–spectroscopy–interaction relationships, offering guidance for the rational design of functionalized GQDs for biosensing and biointerface applications.

2 Computational details

The adsorption of a single amino acid (AA), either glycine or serine, onto pristine and hydroxyl-functionalized, doped GQD surfaces was investigated using Density Functional Theory (DFT) at the M062X/6-31g (d, p) level. Gauss View 6.0 software[33] was used to model and visualize the GQDs. The modeled molecules comprised 9 aromatic benzene rings, with a lateral size of 1.3 nm (Fig. 1). The pristine GQD structure (G) has the formula $C_{31}H_{15}$. The surface was functionalized with a hydroxyl group (-OH) before use as an adsorbent, and the position of the –OH group on the surface was fixed throughout the calculations.

The pristine and functionalized GQD surfaces were doped either singly with boron (B) or nitrogen (N) atoms, or doubly with B and N atoms. First, all modeled structures, including functionalized and doped ones, were subjected to geometry optimizations using Gaussian 2016.[34] The Density Functional Theory (DFT) method[35] was used with the M062X functional[36,37] and a 6-31g (d, p) basis set.[38] The M06-2X functional was selected due to its demonstrated accuracy in describing non-covalent interactions, π-conjugated systems, and hydrogen-bonded complexes without requiring an explicit empirical dispersion correction. Benchmark studies have shown that M06-2X performs reliably for aromatic stacking, adsorption on graphene-like surfaces, and biomolecule–surface interactions, where binding arises from a balance of dispersion, electrostatics, and polarization rather than long-range charge transfer. Furthermore, M06-2X has been widely validated for predicting vibrational properties, making it suitable for combined IR and Raman analysis of functionalized carbon nanostructures.[39–45]

After geometry optimizations, all modified molecules deviated slightly from planarity, particularly at the modification sites (Fig. 2). Harmonic vibrational frequencies were computed to confirm stability, with no imaginary frequencies, thereby

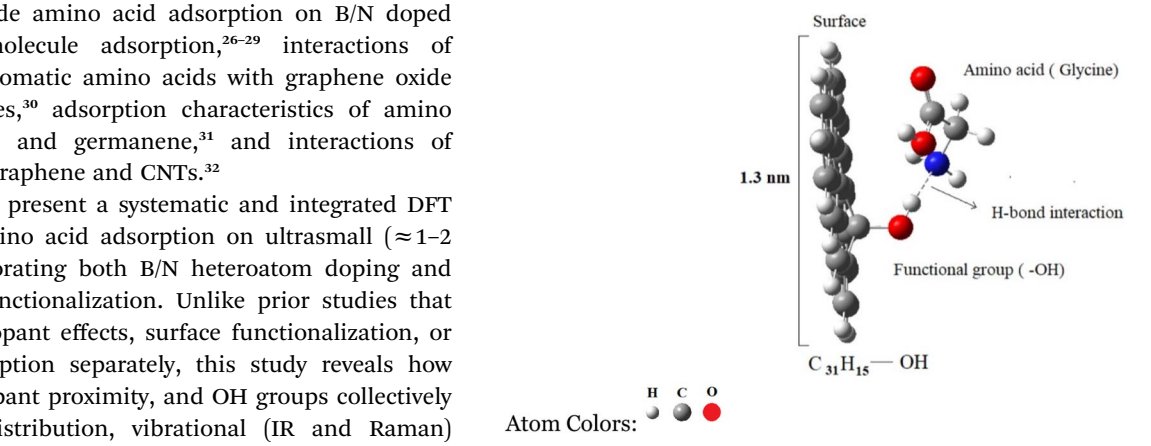

Fig. 1 Side view of the H-bond between the OH-functionalized GQD and AA.

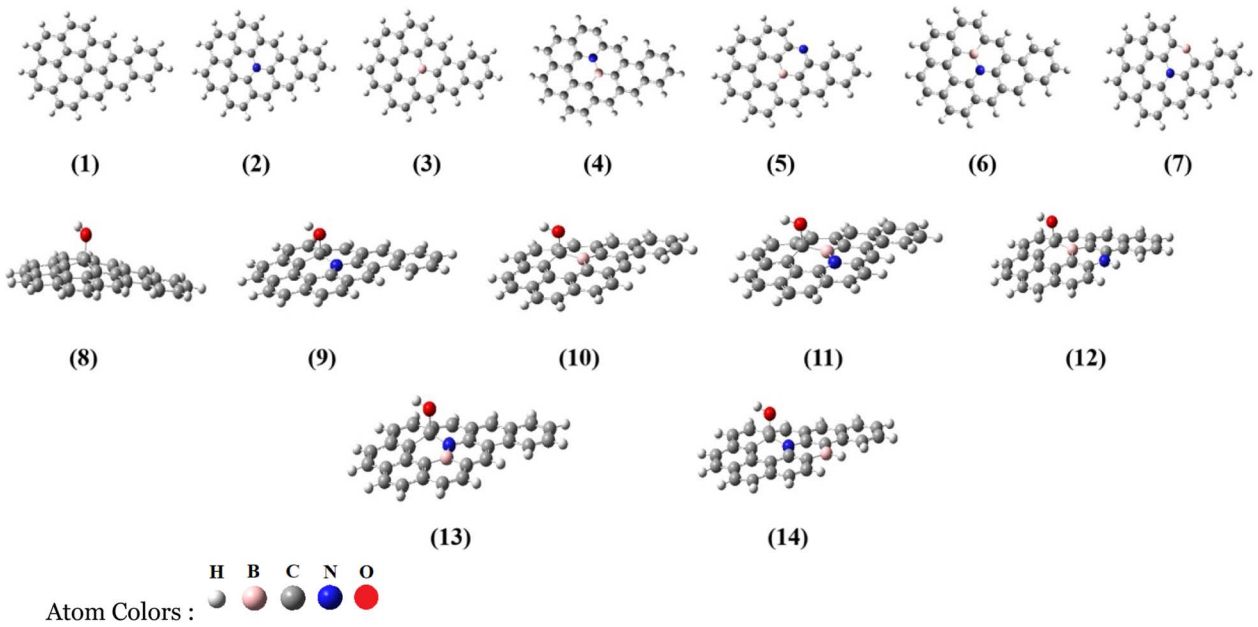

Fig. 2 Optimized structures of pristine, doped and/or functionalized GQDs(1) G, (2) GN, (3) GB, (4) GBN, (5) GBN (2), (6) GNB, (7) GNB (2), (8) G-OH, (9) GN-OH, (10) GB-OH, (11) GBN-OH, (12) GBN (2)-OH, (13) GNB-OH, (14) GNB (2)-OH.

verifying the stationary points. After preparing the surfaces for adsorption studies, the selected amino acids (AAs), glycine (Gly) and serine (Ser), were placed 3.0 Å above the surface along the *z*-direction. Gly and Ser were chosen because they are among the most studied amino acids as adsorbates on graphene-based surfaces.[46–48] The IR and Raman spectra for the systems were obtained. Interaction energies between the surfaces and amino acids were computed and corrected for basis set superposition error (BSSE) using the Counterpoise method.[49] The adsorption energy (E_{ads}) was calculated as the difference between the energy of the non-bonded GQD-AA complex and the energies of the separate molecules, in kcal mol^{-1} (eqn. (1)).

$$E_{ads} = E_{complex} - (E_{GQD} + E_{AA}) \quad (1)$$

3 Results and discussion

3.1 N- and B-doped GQDs

Optimized geometries of boron-doped (GB), boron–nitrogen co-doped (GBN), and (GBN_2), and the relative positions of heteroatom dopants within the GQD framework are illustrated in Fig. S8. In GB, the B atom is located near the central region of the dot, whereas in GBN the B and N atoms occupy adjacent inner carbon sites, forming a B–N pair with a short separation of 1.43 Å. In contrast, in the GBN_2 structure, the B and N dopants are spatially separated (B···N distance of 2.84 Å), leading to a more asymmetric charge distribution. The same structural definitions and nomenclature apply to the corresponding nitrogen-doped and co-doped systems (GN, GNB, and GNB_2).

Fig. 3 depicts the optimized structures of GQD-amino acid complexes. The electronic properties, including total electronic energy, HOMO, and LUMO energies, as well as the LUMO–HOMO band gaps of the complexes, are shown in Table 1. The calculated HOMO–LUMO gaps show clear, systematic modulation upon doping and amino-acid adsorption, reflecting the GQD electronic structure's sensitivity to the local chemical environment. Pristine GQD exhibits a gap of approximately 4.4 eV, consistent with the quantum-confined electronic character of such systems. Nitrogen and boron doping both reduce the bandgap, with singly doped systems showing values between 3.2–3.3 eV, and co-doped or doubly doped systems reaching gaps as low as 3.0 eV. These reductions arise from the introduction of localized dopant states near the frontier orbitals and the accompanying alteration of π-electron distribution. Adsorption of glycine or serine causes only modest changes in the frontier orbital energies, typically within 0.0–0.1 eV, demonstrating that the amino acids interact noncovalently and do not significantly perturb the conjugated backbone of the GQD. Notably, the largest reductions in the gap occur in systems with boron doping or B–N co-doping, consistent with their greater ability to disrupt local aromaticity and introduce acceptor-type states. Overall, the trend indicates that doping is the dominant factor controlling the electronic properties, while biomolecule adsorption produces only subtle electronic perturbations compatible with sensing, recognition, and surface-mediated biochemical interfacing.

The interaction energy analysis shows consistent trends across pristine, doped, and co-doped GQD surfaces, highlighting how chemical modifications affect the adsorption strength of amino acids. For pristine GQD, glycine binds slightly more strongly than serine (−6.2 *vs.* −5.4 kcal mol^{-1}, BSSE-corrected), due to lower deformation costs and minor entropy penalties with glycine. Nitrogen and boron doping systematically increase the adsorption strength for both amino acids, with singly doped systems showing interaction energies

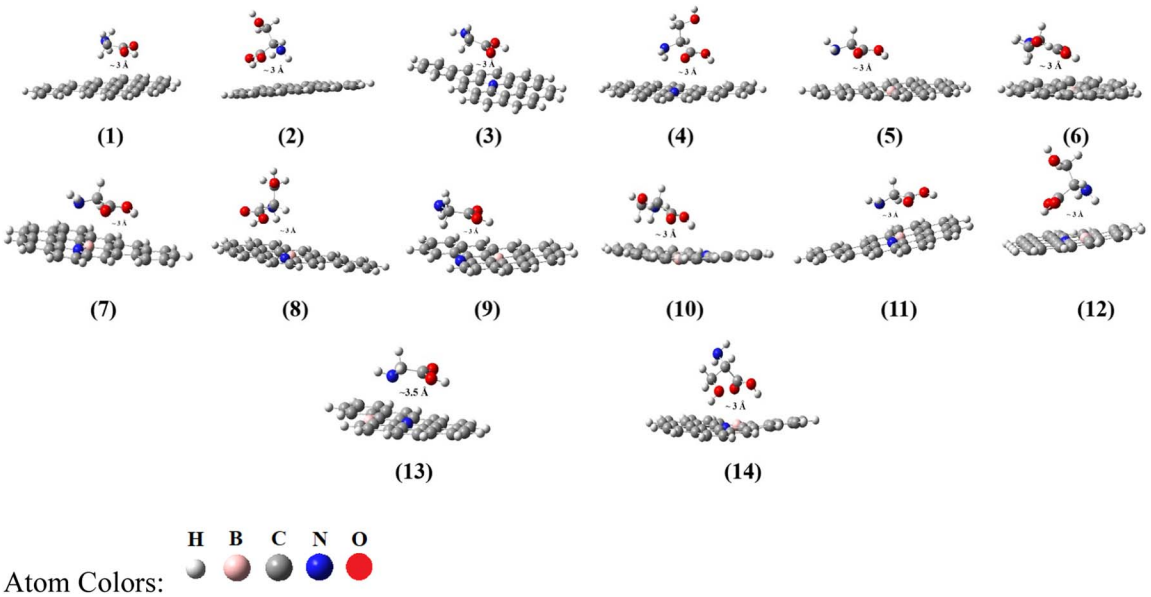

Fig. 3 Optimized structures of AA-adsorbed pristine and doped GQDs. (1) G-Gly, (2) G-Gly, (3) GN-Gly, (4) GN-Ser, (5) GB-Gly, (6) GB-Ser, (7) GBN-Gly, (8) GBN-Ser, (9) GBN(2)-Gly, (10) GBN(2)-Ser, (11) GNB-Gly, (12) GNB-Ser, (13) GNB(2)-Gly, (14) GNB(2)- Ser.

between −7 and −8 kcal mol^{-1} for glycine and −6 to −8 kcal mol^{-1} for serine. Co-doped and doubly doped systems exhibit the strongest interactions, especially GBN_2 and GNB_2, where adsorption energies reach −8.3 to −10.3 kcal mol^{-1} (glycine) and −10.1 to −15.0 kcal mol^{-1} (serine) after correction. These findings indicate that heteroatom addition enhances electrostatic and hydrogen-bonding interactions at the surface, thereby enabling stronger noncovalent binding. Although serine can form extra O–H···O interactions, glycine often exhibits more favorable overall adsorption energies on lightly modified surfaces due to lower enthalpic deformation and minimal entropy loss. However, highly doped systems provide sufficiently strong donor–acceptor and H-bonding environments for serine to fully utilize its additional functional group, thereby improving adsorption in GNB_2 and GBN_2. Overall, the data demonstrate that adsorption strength

Table 1 Electronic properties (E_{HOMO}, E_{LUMO}, band gap (ΔE)), and BSSE-corrected adsorption energies of hydroxyl functionalized complexes in different configurations. ($\Delta E = E_{LUMO} - E_{HOMO}$)[a]

					BSSE corr.	Uncorrected
Complex	E_{HOMO} (in au)	E_{LUMO} (in au)	ΔE (in au)	ΔE (in eV)	E_{ads} (kcal mol^{-1})	E_{ads} (kcal mol^{-1})
Pristine GQG (G)	−0.1898	−0.0293	0.1605	4.4	—	—
GN	−0.1725	−0.0524	0.1201	3.3	—	—
GB	−0.2183	−0.1015	0.1168	3.2	—	—
GNB	−0.18993	−0.03959	0.1503	4.1	—	—
GBN	−0.19045	−0.02901	0.1614	4.4	—	—
GNB_2	−0.1622	−0.0503	0.1119	3.0	—	—
GBN_2	−0.2354	−0.1119	0.1235	3.4	—	—
G-Gly	−0.1931	−0.0330	0.1601	4.4	−6.2	−9.4
G-Ser	−0.1926	−0.0334	0.1593	4.3	−5.4	−9.0
GN-Gly	−0.1773	−0.0561	0.1211	3.3	−8.4	−12.2
GN-Ser	−0.1740	−0.0527	0.1214	3.3	−7.6	−11.3
GB-Gly	−0.2186	−0.0979	0.1208	3.3	−7.9	−12.4
GB-Ser	−0.2255	−0.1074	0.1181	3.2	−7.7	−11.6
GBN-Gly	−0.18828	−0.02503	0.1633	4.4	−7.1	−11.6
GBN-Ser	−0.19356	−0.0319	0.1617	4.4	−6.1	−9.8
GNB-Gly	−0.18474	−0.03626	0.1485	4.0	−6.6	−11.1
GNB-Ser	−0.19059	−0.04185	0.1487	4.0	−6.7	−10.9
GNB_2-Gly	−0.1602	−0.0460	0.1142	3.1	−7.7	−11.7
GNB_2-Ser	−0.1675	−0.0491	0.1184	3.2	−10.3	−15.0
GBN_2-Gly	−0.24036	−0.11451	0.1259	3.4	−8.34	−12.39
GBN_2-Ser	−0.2448	−0.1181	0.1267	3.4	−10.1	−14.4

[a] The GBN and GBN_2 molecules differ in placing the dopant atoms, as do the GNB and GNB_2 molecules.

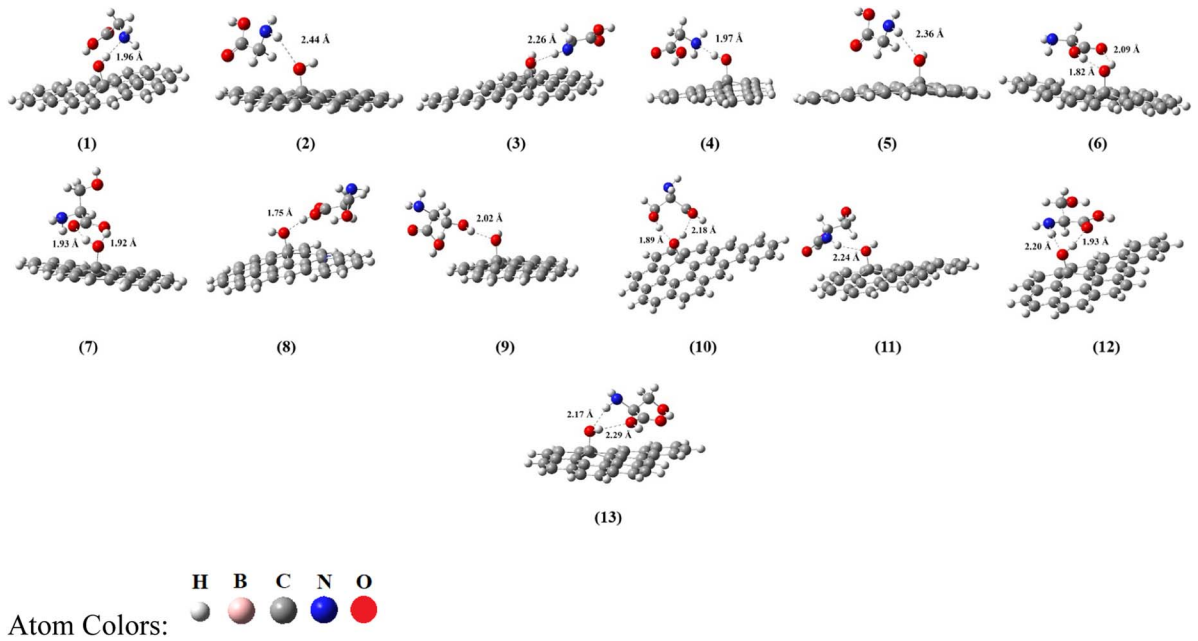

Fig. 4 Optimized structures of amino acid adsorbed, hydroxyl functionalized GQDs. (1) GOH- Gly-1, (2) GOH-Gly-2, (3) GOH-Gly-3, (4) GOH-Gly-4, (5) GOH-Gly-5, (6) GOH-Gly-6, (7) GOH-Ser-1, (8).

depends on dopant type and arrangement, as well as the balance between enthalpic and entropic contributions gained by the surface during amino acid binding.

3.2 Hydroxyl functionalized surface

Graphene, composed of a rigid sp^2-bonded carbon framework, exhibits a largely nonpolar, chemically inert surface that interacts weakly with polar adsorbates. Covalent functionalization with polar groups, such as hydroxyls, enhances the surface's affinity for hydrogen bonding and dipolar interactions but simultaneously disrupts π-conjugation. Hydroxylation of the GQD increases the HOMO–LUMO gap by 0.4 eV, consistent with the introduction of local sp^3 defects and distortions in electron density; this effect is expected to diminish with increasing graphene size due to reduced relative perturbation. To explore the adsorption behavior of amino acids on hydroxylated GQD, six initial orientations of glycine and seven of serine were placed 3.0 Å above the surface and fully optimized. These configurations differ only in their initial rotational placement relative to the functional groups on the GQD. Fig. 4 shows the resulting geometries and the key hydrogen-bond distances. In Table 2, the adsorption energies of the studies amino acids are presented. Although adsorption of a single amino acid does not significantly alter the electronic properties of the GQD surface, BSSE-corrected adsorption energies vary by up to 10.0 kcal mol^{-1} depending on the amino acid conformation. Among all structures, GOH-Gly- 6 emerged as the most stable, with an interaction energy of −16.2 kcal mol^{-1}, stabilized by a cooperative six-membered hydrogen-bonded ring involving double

Table 2 E_{HOMO}, E_{LUMO}, ΔE, and adsorption energies of hydroxyl functionalized complexes in different configurations. ($\Delta E = E_{LUMO} - E_{HOMO}$)

Complex	E_{HOMO} (in au)	E_{LUMO} (in au)	ΔE (in au)	ΔE (in eV)	BSSE corrected adsorption energy (kcal mol^{-1})	Uncorrected assorption energy (kcal mol^{-1})
GOH	−0.2329	−0.0575	0.1753	4.8	—	—
GOH-Gly 1	−0.2299	−0.0553	0.1746	4.8	−13.6	−18.4
GOH-Gly 2	−0.2358	−0.0606	0.1752	4.8	−6.4	−9.8
GOH-Gly 3	−0.2337	−0.0581	0.1756	4.8	−7.3	−11.2
GOH-Gly 4	−0.2301	−0.0549	0.1753	4.8	−13.1	−17.8
GOH-Gly 5	−0.2355	−0.0602	0.1753	4.8	−6.1	−9.8
GOH-Gly 6	−0.2377	−0.0636	0.1742	4.7	−16.2	−22.5
GOH-Ser 1	−0.2353	−0.0603	0.1750	4.8	−14.6	−20.6
GOH-Ser 2	−0.2388	−0.0637	0.1751	4.8	−12.9	−18.0
GOH-Ser 3	−0.2364	−0.0608	0.1756	4.8	−7.5	−11.6
GOH-Ser 4	−0.2416	−0.0672	0.1743	4.7	−11.4	−16.9
GOH-Ser 5	−0.2375	−0.0620	0.1755	4.8	−8.4	−12.6
GOH-Ser 6	−0.2369	−0.0612	0.1757	4.8	−10.5	−15.5
GOH-Ser 7	−0.2373	−0.0633	0.1740	4.7	−10.5	−16.9

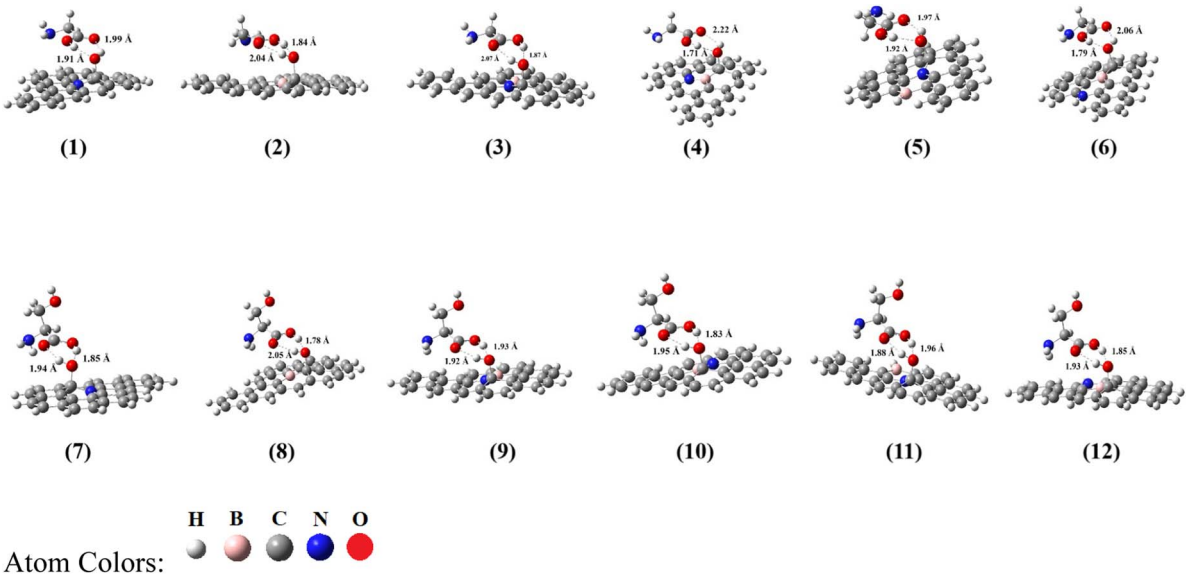

Fig. 5 Optimized structures of amino Aacid adsorbed on hydroxyl functionalized and doped GQDs. (1) GN-OH-Gly, (2) GB-OH-Gly, (3) GNB-OH-Gly, (4) GBN-OH-Gly, (5) GNB(2)-OH-Gly, (6) GBN_2-OH-Gly, (7) GN-OH-Ser, (8) GB-OH - Ser, (9) GNB-OH - Ser, (10) GBN-OH - Ser, (11) GNB(2)-OH - Ser, (12) GBN_2-OH - Ser.

O–H···O interactions between the surface hydroxyls and glycine. For serine, the most favorable structure was GOH-Ser-1, featuring a short O–H···O hydrogen bond of 1.75 Å and an adsorption energy of −14.6 kcal mol^{-1}, in good agreement with literature values (∼−13.2 kcal mol^{-1}).[25] The next most stable glycine conformation, GOH-Gly-1, exhibits a single O–H···N interaction with an energy of −13.6 kcal mol^{-1}.[50] Although serine offers more potential binding motifs due to its additional side-chain hydroxyl, glycine consistently exhibits slightly stronger adsorption on the hydroxylated surface, with the most stable glycine and serine geometries differing by ∼1.6 kcal mol^{-1}. Several conformers (GOH-Gly-2, 3, 5 and GOH-Ser-3, 5) showed minimal binding and were therefore excluded from further analysis. Based on these stability trends, GOH- Gly- 6 and GOH-Ser-1 were selected as representative adsorption geometries for subsequent electronic and spectroscopic calculations.

3.3 N- and B-doped, hydroxyl functionalized GQDs

The optimized structures of the amino acid adsorbed, doped, and hydroxyl-functionalized GQDs are shown in Fig. 5. While

Table 3 E_{HOMO}, E_{LUMO}, ΔE, and adsorption energies of amino acid adsorption on hydroxyl functionalized and doped complexes ($\Delta E = E_{LUMO} - E_{HOMO}$)

Complex	E_{HOMO} (au)	E_{LUMO} (au)	ΔE (au)	ΔE (eV)	BSSE corrected adsorption energy (kcal mol^{-1})	Uncorrected assorption energy (kcal mol^{-1})
GOH	−0.2329	−0.0575	0.1753	4.8	—	—
GB-OH	−0.2209	−0.0514	0.1694	4.6	—	—
GN-OH	−0.1677	−0.0416	0.126	3.4	—	—
GBN-OH	−0.2221	−0.05	0.1721	4.7	—	—
GNB-OH	−0.2409	−0.0608	0.1802	4.9	—	—
GBN(2)-OH	−0.2272	−0.0463	0.1808	4.9	—	—
GNB(2)-OH	−0.2448	−0.0576	0.1872	5.1	—	—
GB-OH-Gly	−0.2168	−0.0499	0.1668	4.5	−16.5	−23.1
GNB-OH-Gly	−0.23951	−0.0595	0.18	4.9	−16.4	−22.9
GNB(2)-OH-Gly	−0.24707	−0.06068	0.1864	5.1	−13.8	−19.4
GBN(2)-OH-Gly	−0.2267	−0.0475	0.1793	4.9	−14.4	−20.8
GBN-OH-Gly	−0.2229	−0.05	0.1728	4.7	−15.1	−21.6
GN-OH-Gly	−0.1672	−0.0382	0.1289	3.5	−13.6	−20.0
GB-OH-Ser	−0.224	−0.0543	0.1697	4.6	−15.0	−20.9
GBN(2)-OH-Ser	−0.2293	−0.0499	0.1795	4.9	−14.2	−20.1
GBN-OH-Ser	−0.2252	−0.0526	0.1727	4.7	−14.3	−20.2
GN-OH-Ser	−0.1703	−0.0426	0.1277	3.5	−11.6	−16.5
GNB(2)-OH-Ser	−0.2454	−0.0583	0.1871	5.1	−15.2	−21.3
GNB-OH-Ser	−0.2428	−0.0631	0.1798	4.9	−15.0	−20.9

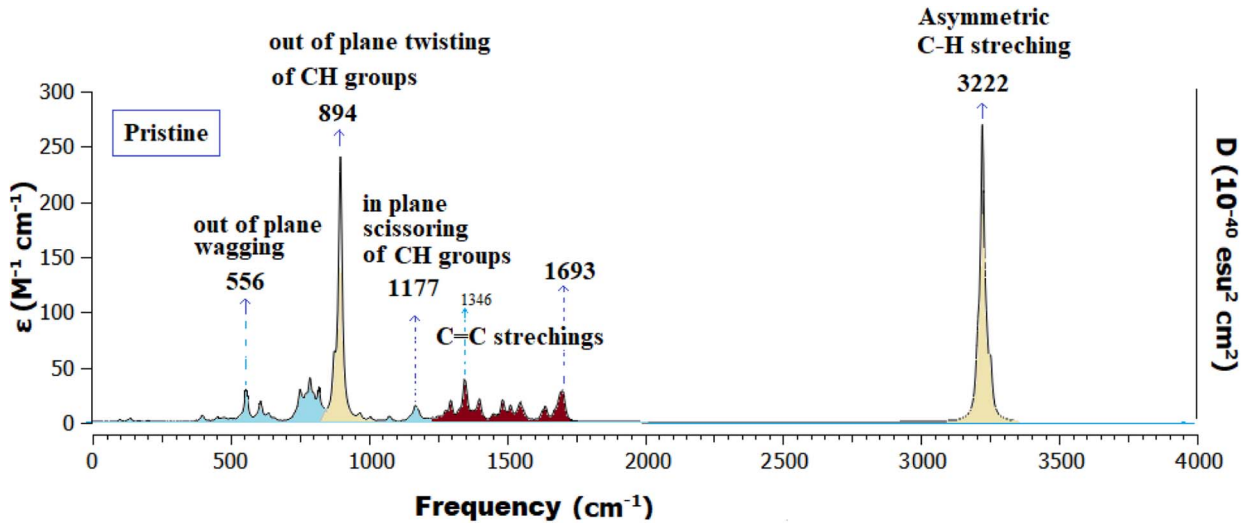

Fig. 6 IR spectrum of pristine GQD (G). Frequencies are given in wavenumbers, cm^{-1}.

the interaction energies obtained from the doped and functionalized systems are consistently larger than those of the pristine and doped systems, they are not always more favorable than those of the solely functionalized systems (Table 3). Generally, B doping increases the interaction energy in magnitude, while N doping decreases it. This observation, along with the other results in Table 6, typically aligns with findings in the literature.[24,25] Incorporating two dopant atoms, N and B, onto the same surface does not always yield better results than the singly doped systems. The positions of the dopant atoms on the surface relative to one another play a crucial role in stabilizing or destabilizing the π-electron density. Replacing terminal carbon atoms with dopant atoms is less preferable than replacing inner carbon atoms in Gly-adsorbed GQDs, whereas this effect was not observed in Ser-adsorbed systems.

3.4 IR and Raman spectroscopic analyses

IR and Raman spectroscopic analyses were conducted to identify changes in bands associated with hydrogen bonding on hydroxyl-functionalized and B, N-doped GQD surfaces. The data collected in this study may assist experimentalists in confirming the physical adsorption of molecules onto the synthesized graphene surfaces. Fig. 6 presents the IR spectrum of pristine graphene, aiding in interpreting relative changes in IR frequencies caused by surface modifications. Significant peaks associated with vibrational modes and their wavenumbers are indicated on the plot. The IR spectra of all the structures examined in detail are included in the SI.

In Tables 4–6, we present the calculated IR frequencies (in cm^{-1}) for the O–H (ν_1), N–H (ν_2), and C=O (ν_3) stretching modes. The most significant changes occur in the modes associated with H-bond formation between surface atoms and amino acids.

Analyzing the data in Table 4 reveals that doping significantly affects vibrational signatures, with B-containing surfaces exhibiting the most pronounced red shifts, indicating stronger hydrogen bonds and increased surface reactivity. Serine exhibits a stronger binding than glycine, as shown by consistently larger red-shifts in ν_1 and ν_3. These combined trends confirm that doping improves adsorption strength, and the effect varies with dopant position, with some configurations (*e.g.*, GNB, GBN, GNB_2) causing noticeably greater perturbations.

Table 4 Calculated IR Frequencies (unscaled) of B, N-Doped Graphene (G)-Amino acid complexes

Complex	ν_1(O–H) (cm^{-1})	ν_2(N–H) (cm^{-1})	ν_3(C=O) (cm^{-1})
Pristine G-Gly	3804	3529 (*sym*)	1896
		3605 (*asym*)	
Pristine G-Ser	3764	3512 (*sym*)	1881
	3916	3614 (*asym*)	
GN-Gly	3795	3533 (*sym*)	1884
		3621 (*asym*)	
GN-Ser	3754	3519 (*sym*)	1869
	3913	3616 (*asym*)	
GB-Gly	3777	3530 (*sym*)	1894
		3637 (*asym*)	
GB-Ser	3742	3526 (*sym*)	1845
	3811	3622 (*asym*)	
GNB-Gly	3812	3554 (*sym*)	1896
		3656 (*asym*)	
GNB-Ser	3770	3519 (*sym*)	1872
	3914	3614 (*asym*)	
GBN-Gly	3810	3552 (*sym*)	1897
		3654 (*asym*)	
GBN-Ser	3770	3524 (*sym*)	1882
	3911	3621 (*asym*)	
GNB_2-Gly	3805	3547 (*sym*)	1910
		3640 (*asym*)	
GNB_2-Ser	3678	3520 (*sym*)	1858
	3875	3613 (*asym*)	
GBN_2-Gly	3793	3530 (*sym*)	1885
		3606 (*asym*)	
GBN_2-Ser	3748	3527 (*sym*)	1848
	3832	3615 (*asym*)	

The vibrational data in Table 5 show that adsorption of glycine and serine on hydroxylated graphene (GOH) consistently alters the O–H, N–H, and C=O stretching modes. The size and direction of these shifts depend on the type and strength of hydrogen bonds formed at each adsorption geometry. In most complexes, ν_1(O–H) experiences notable red-shifts (3380–3800 cm^{-1}) compared to GOH (3835 cm^{-1}), especially when the surface O–H group donates a hydrogen bond to the amino acid's N–H or O–H group. The largest red-shifts (such as GOH-Gly6, GOH-Ser2, GOH-Ser4) are associated with dual hydrogen bonding or stronger O–H···O interactions, indicating increased polarization of the surface hydroxyl groups.

The N–H stretching frequencies (ν_2) stay mostly steady but shift consistently by 10–20 cm^{-1} depending on whether N–H acts as an H-bond acceptor or donor. Complexes with bidirectional hydrogen bonding (surface O–H ↔ N–H or O–HAA) exhibit the most notable changes, indicating stronger interaction geometries.

The C=O stretching mode (ν_3) ranges from 1831 to 1921 cm^{-1}, with serine complexes generally showing lower ν_3 values than glycine, indicating stronger stabilization of the carboxyl group. The highest C=O frequency (1921 cm^{-1} in GOH-Ser5) corresponds to a configuration where the carbonyl acts as a hydrogen-bond acceptor, which increases its bond polarization.

The hydrogen-bond assignments confirm that glycine mainly interacts through N–H···O(H) surface interactions, with occasional O–H···O(H) bonds in more stable configurations. Serine shows a wider variety of binding motifs, including O–H···O(H), N–H···O(H), and O–H···O=C interactions, due to its additional side-chain hydroxyl group. It forms multiple simultaneous hydrogen bonds more consistently than glycine, which explains its greater impact on the ν_1 and ν_3 values.

Overall, Table 5 shows that GOH surfaces can support a wide range of hydrogen-bonding geometries and that serine exhibits stronger, more complex adsorption than glycine, as evidenced by both spectral shifts and bonding patterns.

The vibrational data in Table 6 show that B- and N-doped GOH surfaces engage in strong dual O–H···O hydrogen bonding with both glycine and serine, producing systematic red-shifts in the O–H, N–H, and C=O stretching modes. The surface O–H stretching frequencies decrease markedly (from ~3835 cm^{-1} in GOH to 3260–3580 cm^{-1} across complexes),

Table 5 Calculated IR Frequencies (unscaled) of GOH-Amino acid complexes

Complex	ν_1(O–H) (cm^{-1})	ν_2(N–H) (cm^{-1})	ν_3(C=O) (cm^{-1})	H-bond formed between
GOH	3835	—	—	—
Gly (free)	3834	3552 (*sym*) 3645 (*asym*)	1921	$(O–H)_{surface}$–$(N–H)_{Gly}$
GOH-Gly 1	3523 3782	3545 (*sym*) 3632 (*asym*)	1899	$(O–H)_{surface}$–$(N–H)_{Gly}$
GOH-Gly 2	3833	3533 (*sym*) 3628 (*asym*)	1894	$(O–H)_{surface}$–$(N–H)_{Gly}$
GOH-Gly 3	3826 3835	3523 (*sym*) 3629 (*asym*)	1905	$(H–O)_{surface}$–$(N–H)_{Gly}$
GOH-Gly 4	3558 3766	3529 (*sym*) 3624 (*asym*)	1897	$(O–H)_{surface}$–$(N–H)_{Gly}$
GOH-Gly 5	3832 3833	3542 (*sym*) 3642 (*asym*)	1896	$(H–O)_{surface}$–$(N–H)_{AA}$
GOH-Gly 6	3465 3713	3543 (*sym*) 3631 (*asym*)	1853	$(O–H)_{surface}$–$(O–H)_{Gly}$ $(H–O)_{surface}$–$(H–O)_{Gly}$
GOH-Ser 1	3548 3650 3912	3527 (*sym*) 3624 (*asym*)	1831	$(O–H)_{surface}$–$(O–H)_{Ser}$ $(H–O)_{surface}$–$(N–H)_{Ser}$
GOH-Ser 2	3387 3841 3850	3545 (*sym*) 3640 (*asym*)	1883	$(H–O)_{surface}$–$(H–O)_{Ser}$
GOH-Ser 3	3786 3810 3815	3552 (*sym*) 3648 (*asym*)	1892	$(H–O)_{surface}$–$(H–O)_{Ser}$
GOH-Ser 4	3747 3755 3807	3525 (*sym*) 3609 (*asym*)	1872	$(O–H)_{surface}$–$(O–H)_{Ser}$ $(H–O)_{surface}$–$(H–O)_{Ser}$
GOH-Ser 5	3817 3824 3887	3525 (*sym*) 3625 (*asym*)	1921	$(H–O)_{surface}$–$(H–N)_{Ser}$
GOH-Ser 6	3736 3796 3888	3535 (*sym*) 3629 (*asym*)	1887	$(H–O)_{surface}$–$(H–N)_{Ser}$ $(O–H)_{surface}$–$(O=C)_{Ser}$
GOH-Ser 7	3796 3813 3829	3521 (*sym*) 3604 (*asym*)	1862	$(H–O)_{surface}$–$(H–N)_{Ser}$ $(O–H)_{surface}$–$(O–H)_{Ser}$

demonstrating significant weakening and elongation of the surface hydroxyl bonds due to strong O–H···O interactions. The largest red-shifts appear in GBN–OH–Gly (3261 cm^{-1}) and several serine complexes, indicating that B-containing doped sites promote the strongest hydrogen-bond formation.

The N–H stretching modes of the amino acids remain relatively stable but shift slightly depending on substituent environment, consistent with their role mainly as hydrogen-bond donors rather than primary acceptors. In contrast, the C═O stretching frequencies show consistent downshifts for serine (1822–1835 cm^{-1}) relative to glycine (1850–1865 cm^{-1}), indicating stronger carbonyl participation in serine complexes. This reflects serine's ability to form more extensive and cooperative hydrogen-bond networks due to its additional side-chain hydroxyl group.

Across all systems, we observed that all complexes form double O–H···O hydrogen bonds, stabilizing the adsorbed amino acid. B-doped surfaces (GB, GBN, GNB) show deeper O–H red-shifts, stronger H-bonding and greater surface polarization. Serine consistently produces lower C═O frequencies than glycine, confirming stronger binding and greater electron density redistribution. Dual hydrogen bonding is a universal interaction motif for both glycine and serine across all doped surfaces.

Overall, these IR trends demonstrate that heteroatom doping amplifies hydrogen-bond strength, particularly at boron sites, and that serine binds more strongly than glycine due to its additional hydroxyl group enabling more cooperative interactions.

The Raman spectra (Fig. 7) show a clear progression in structural changes from pristine graphene to OH-functionalized and amino-acid-attached surfaces. Pristine graphene displays the expected sharp D and G bands, indicating a well-maintained sp^2 network. After OH functionalization, both bands broaden, and the D-band intensity grows, reflecting defect creation and disruption of π-conjugation due to covalent C–O bonding. In contrast, adsorption of glycine and serine results in only minor spectral changes: the D and G bands stay largely the same from G-OH, confirming that the graphene lattice remains unaltered chemically. Instead, small new features appear in the 1200–1700 cm^{-1} range, matching amino-acid vibrational modes, with serine showing a slightly richer pattern because of its extra hydroxyl group. These trends indicate that, while OH groups cause permanent lattice modifications, amino acids interact *via* noncovalent forces, preserving the original Raman signature of graphene.

The Raman spectra of doped graphene systems (Fig. 8) show that the arrangement of B and N atoms greatly affects the lattice's

Table 6 Calculated IR frequencies (unscaled) of OH functionalized and B, N-doped G-amino acid complexes

Complex	O–H streching (cm^{-1})	N–H streching (cm^{-1})	C═O streching (cm^{-1})	H bond formed between
Gly (free)	3834	3552 (*sym*) 3645 (*asym*)	1921	(O–H)surface – (O–H)Gly (double)
GB-OH-Gly	3431 3704	3545 (*sym*) 3639 (*asym*)	1863	(O–H)surface – (O–H)Gly (double)
GBN_2- OH-Gly	3377 3694	3546 (*sym*) 3639 (*asym*) 3677 (edge)	1863	(O–H)surface – (O–H)Gly (double)
GBN-OH-Gly	3261 3749	3549 (*sym*) 3641 (*asym*)	1865	(O–H)surface – (O–H)Gly (double)
GN-OH-Gly	3547 3695	3550 (*sym*) 3643 (*asym*)	1864	(O–H)surface – (O–H)Gly (double)
GB-OH-Ser	3379 3727 3915	3509 (*sym*) 3609 (*asym*)	1822	(O–H)surface – (O–H)Ser (double)
GBN_2- OH-Ser	3450 3670 3912	3522 (*sym*) 3621 (*asym*) 3677 (edge)	1834	(O–H)surface – (O–H)Ser (double)
GBN-OH-Ser	3459 3663 3913	3525 (*sym*) 3620 (*asym*)	1835	(O–H)surface – (O–H)Ser (double)
GN-OH-Ser	3504 3654 3915	3518 (*sym*) 3614 (*asym*)	1834	(O–H)surface – (O–H)Ser (double)
GNB_2-OH-Ser	3577 3631 3912	3530 (*sym*) 3625 (*asym*)	1828	(O–H)surface – (O–H)Ser (double)
GNB-OH-Ser	3576 3637 3912	3529 (*sym*) 3626 (*asym*)	1829	(O–H)surface – (O–H)Ser (double)
GNB-OH-Gly	3533 3713	3535 (*sym*) 3640 (*asym*)	1850	(O–H)surface – (O–H)Gly (double)
GNB-OH-2-Gly	3586 3669	3545 (*sym*) 3646 (*asym*)	1858	(O–H)surface – (O–H)Gly (double)

vibrational response. GNB and GBN display unique spectral features, especially in the 1400–1600 cm^{-1} range, where variations in intensity and peak shape indicate asymmetric charge redistribution caused by B–N positional inversion. Low-frequency modes below 1000 cm^{-1} also differ between the two structures, suggesting that dopant placement impacts out-of-plane lattice distortions. After OH functionalization, both doped systems clearly show signs of covalent modification, including new C–O stretching modes and an O–H band near 3200–3600 cm^{-1}. Still, the extent of spectral change depends on dopant location: GNB-OH displays stronger C–O activity and broader spectral features, while GBN_OH shows sharper, more shifted peaks and increased low-frequency bending modes. These findings indicate that both the intrinsic position of the heteroatoms and subsequent OH functionalization influence the vibrational properties of the doped graphene, resulting in distinct Raman signatures for each configuration.

The Raman spectra of G, GN, and GB (Fig. 9) exhibit the characteristic features of graphene-based systems, namely the D

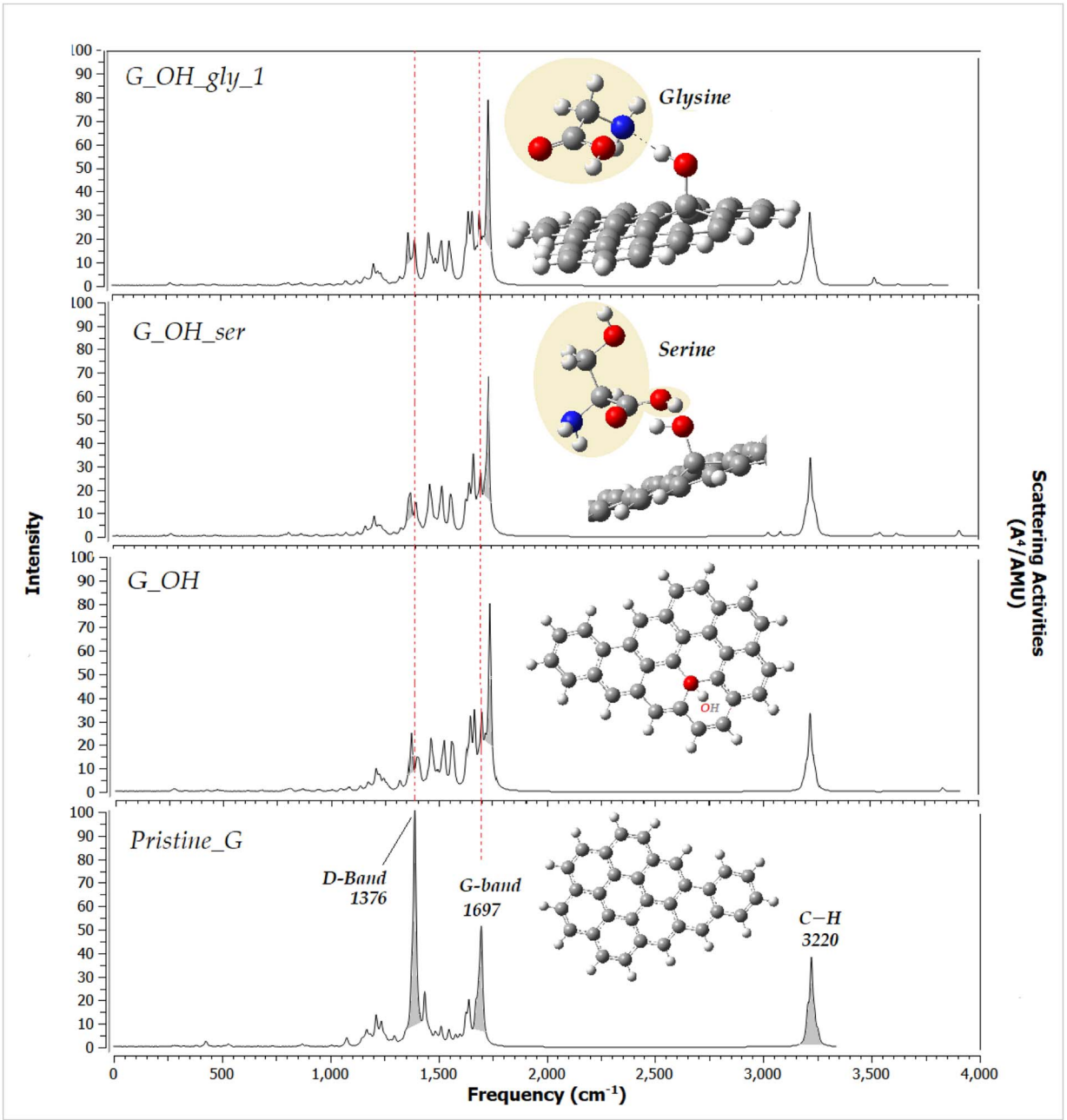

Fig. 7 Raman activity spectra of pristine graphene (G), OH functionalized G (G-OH), serine and glycine adsorbed functionalized graphene surface (G-OH-gly, G-OH-ser).

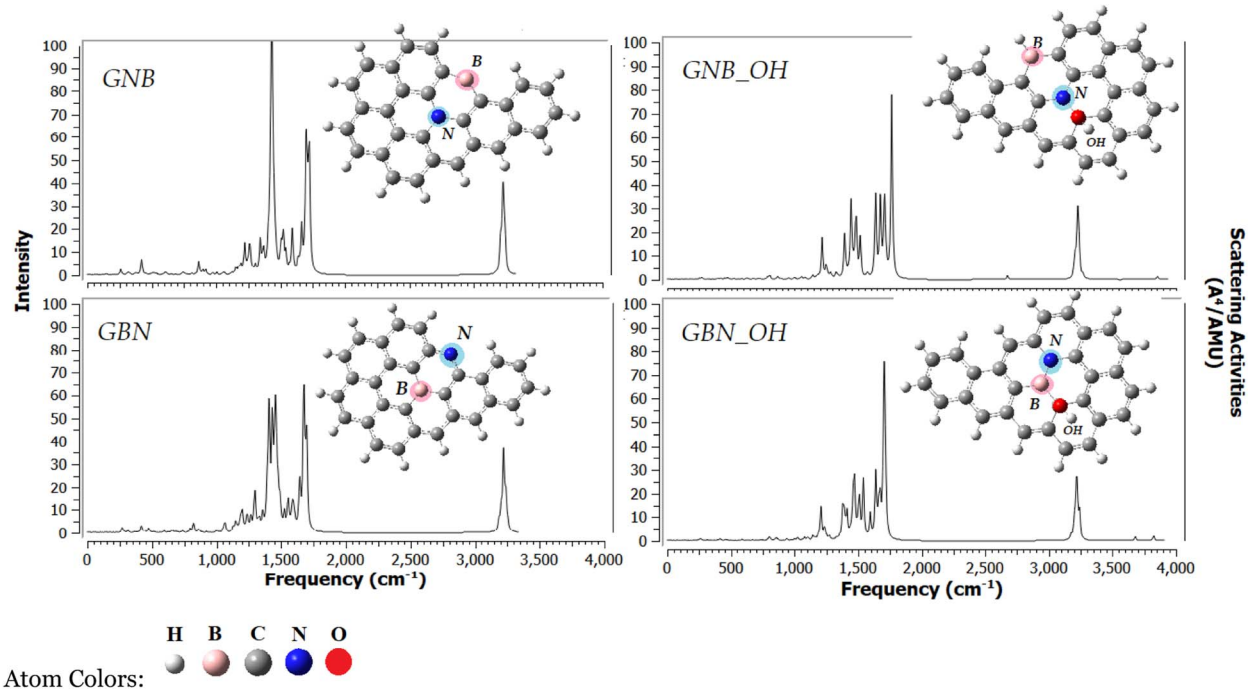

Fig. 8 Raman activity spectra of B–N doubly doped and OH functionalized G.

band (~1350 cm^{-1}), G band (~1580–1600 cm^{-1}), and 2D band (~2700–3000 cm^{-1}). Heteroatom doping significantly modifies the relative intensities of these bands. Nitrogen doping (GN) results in a slightly enhanced D band and subtle shifts in the G band, indicating increased defect sites and changes in the electronic structure. Boron doping (GB) produces an even more

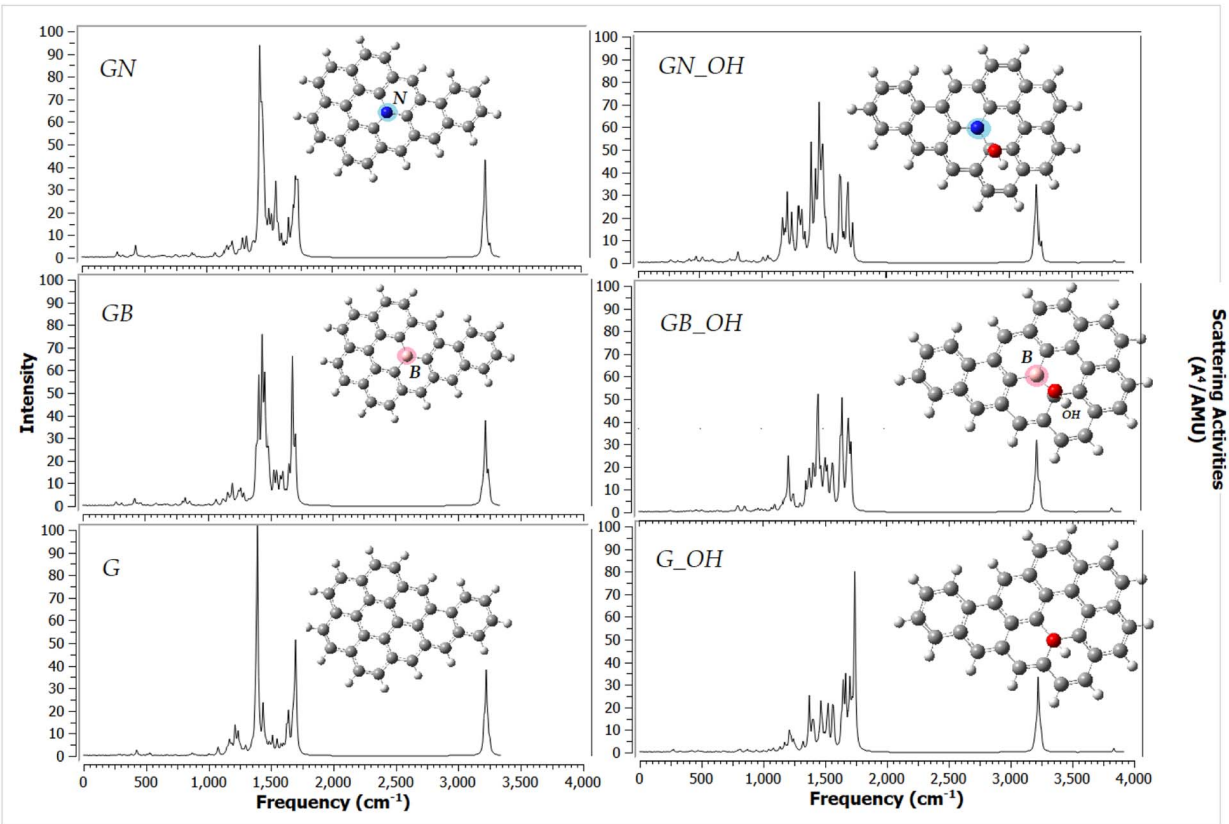

Fig. 9 Raman activity spectra of B or N-doped G before and after OH functionalization.

pronounced increase in the D-band intensity, along with broadening of both D and G bands, consistent with greater lattice distortion caused by B substitution. Upon hydroxylation (GN-OH, GB-OH, G-OH), the spectra show more dramatic changes: the D band becomes stronger, while several features in the 1000–1600 cm^{-1} region either shift or decrease in intensity, reflecting increased disorder and local sp^2-to-sp^3 rehybridization due to OH attachment. The O–H functionalization also partially suppresses or attenuates the 2D band, especially in GB-OH, indicating that boron-containing structures undergo the most significant structural perturbation. Overall, N and B dopants primarily alter the degree of disorder, whereas hydroxylation introduces additional defects and significantly alters both band positions and intensities.

Boron doping causes significantly more lattice distortion in graphene compared to nitrogen, and this is clearly shown in the Raman spectra. Although both dopants introduce defects, the GB and especially GB-OH spectra show stronger and broader features in the 1000–1600 cm^{-1} range and a more prominent D band, indicating greater structural disorder. This difference arises from the atomic and electronic properties of the dopants: boron has a larger atomic radius and is electron-deficient relative to carbon, resulting in longer, weaker B–C bonds that break up the π-conjugated network. On the other hand, nitrogen is similar in size to carbon and forms stronger C–N bonds, which helps the lattice keep much of its structure. As a result, boron substitution causes more geometric strain and disturbs aromatic ring vibrations, especially after hydroxylation.

The IR and Raman spectroscopic analyses further support the adsorption of amino acids on the pristine, doped, and hydroxyl-functionalized GQD surfaces. For the hydroxylated structures, the formation of dual hydrogen bonds between the –OH groups and the functional groups of glycine or serine results in clear red shifts in the O–H and N–H stretching modes, indicating enhanced intermolecular interactions. Doped systems exhibit more pronounced perturbations in vibrational features, with the introduction of B and N atoms modulating local electron densities and shifting characteristic C=C and C–O vibrational bands. These dopant-induced changes alter the polarizability of the π-framework, producing Raman peak shifts that align with increased charge transfer upon adsorption. Notably, double-doped GNB_2 and GBN_2 surfaces display the most significant spectral variations, correlating with their larger interaction energies and lower HOMO–LUMO gaps. Overall, the combined IR and Raman findings confirm that doping and functionalization not only enhance amino acid adsorption but also significantly influence the vibrational response of the GQD framework, reflecting the electronic and structural reorganization caused by surface–molecule interactions.

4 Conclusion

This DFT study demonstrates that surface functionalization and heteroatom doping play decisive roles in tuning the electronic and vibrational properties of graphene quantum dots. B and N doping reduces the HOMO–LUMO gap—by nearly 1 eV in some configurations—with the strongest effects observed when dopants are positioned at the edges. Hydroxyl functionalization introduces covalent defects that markedly alter both IR and Raman features, while amino acid adsorption produces characteristic vibrational signatures without disrupting the underlying graphene lattice. Raman spectra further indicate that boron doping and hydroxylation induce the largest structural distortions, whereas nitrogen incorporation and amino-acid binding introduce comparatively subtle perturbations.

Interaction energy analysis shows that both singly and doubly doped GQDs enhance amino acid adsorption, providing binding strengths sufficient for stable attachment yet weak enough to preserve physisorption and enable controlled release. The observed IR and Raman shifts—particularly in O–H, N–H, and C=O stretching regions, as well as changes in the D and G bands—confirm that these modified GQD surfaces readily form noncovalent hydrogen-bonding and charge–transfer interactions with glycine and serine. These vibrational signatures also serve as reliable spectroscopic markers for successful surface functionalization.

Overall, our results highlight the high tunability of GQDs through targeted doping and chemical modification and demonstrate their potential as versatile nanoscale platforms for the adsorption of small biomolecules, including amino acids and drug-like species, supporting future applications in sensing, delivery, and biointerface design.

The present work provides detailed insights into the effects of heteroatom doping, surface functionalization, and amino acid adsorption on graphene quantum dots. It relies on finite GQD models and static DFT calculations performed in the gas phase or in an implicit solvent framework. However, dynamic effects, temperature contributions, and explicit solvent interactions were not considered and may influence adsorption strengths and vibrational features under experimental conditions.

In this study, the DFT investigations were restricted to solid-state models involving ultra-small, non-periodic surfaces with no imposed symmetry. Although such models capture the essential local interactions, their experimental synthesis and direct characterization remain highly challenging. Future studies may therefore extend the calculations to physiologically relevant conditions by incorporating aqueous environments through continuum solvation models or explicit solvent treatments within DFT and molecular dynamics frameworks. In addition, the effects of pH and temperature on adsorption behavior can be systematically explored, enabling a more realistic description of amino acid–surface interactions under experimental and biological conditions.

Conflicts of interest

There are no conflicts to declare.

Data availability

The data supporting this article are included in the supplementary information (SI). Supplementary information: theoretical IR spectra (Fig. S1–S7) of all the studied GQD systems, which include detailed analyses of the vibrational modes (Tables S1–S7)

with interpretations of the vibrational shifts caused by surface covalent and non-covalent modifications. The figure showing the lattice positions of the dopant atoms is provided in Fig. S8, along with an explanation. See DOI: https://doi.org/10.1039/d6ra00110f. Additional data, if needed, are available from the corresponding author upon request.

Acknowledgements

We acknowledge the computer time provided by the National High-Performance Computing Center (UHEM) under grant number 5004452017.

References

1 L. A. Falkovsky, Optical properties of graphene, *J. Phys.: Conf. Ser.*, 2008, **129**, 012004.
2 S. Gurunathan and J. Kim, Synthesis, toxicity, biocompatibility, and biomedical applications of graphene and graphene-related materials, *Int. J. Nanomed.*, 2016, **11**, 1927–1945, DOI: 10.2147/IJN.S105264, [Online] Available: https://www.ncbi.nlm.nih.gov/pmc/articles/PMC4863686/.
3 K. Yang, L. Feng and Z. Liu, Stimuli-responsive drug delivery systems based on nano-graphene for cancer therapy, *Adv. Drug Delivery Rev.*, 2016, **105**(Part B), 228–241, DOI: 10.1016/j.addr.2016.05.015, [Online] Available: https://pubmed.ncbi.nlm.nih.gov/27233212/.
4 B. Zhang, Y. Wang and G. Zhai, Biomedical applications of graphene-based materials, *Mater. Sci. Eng. C*, 2016, **61**, 953–964, DOI: 10.1016/j.msec.2015.12.073, [Online] Available: https://pubmed.ncbi.nlm.nih.gov/26838925/.
5 G. Shim, M. Kim, J. Y. Park and Y. Oh, Graphene-based nanosheets for delivery of chemotherapeutics and biological drugs, *Adv. Drug Delivery Rev.*, 2016, **105**, 205–227, DOI: 10.1016/j.addr.2016.04.004, [Online] Available: https://www.sciencedirect.com/science/article/abs/pii/S0169409X1630103X.
6 P. A. Rasheed, M. Ankitha, V. K. Pillai and S. Alwarappan, Graphene quantum dots for biosensing and bioimaging, *RSC Adv.*, 2024, **14**, 16001–16023.
7 N. Sohal, B. Maity and S. Basu, Recent advances in heteroatom-doped graphene quantum dots for sensing applications, *RSC Adv.*, 2021, **11**, 25586–25615.
8 S. Radhakrishnan, J. Lee, R. Jaumann, *et al.*, Recent advances in graphene quantum dot-based optical and electrochemical (bio)analytical sensors, *Mater. Adv.*, 2021, **2**, 1234–1258.
9 V. Georgakilas, *et al.*, Functionalization of graphene: covalent and noncovalent approaches, derivatives and applications, *Chem. Rev.*, 2012, **112**(11), 6156–6214, DOI: 10.1021/cr3000412.
10 Y. Si and E. T. Samulski, Synthesis of water-soluble graphene, *Nano Lett.*, 2008, **8**, 1679–1682, DOI: 10.1021/nl080604h.
11 D. R. Dreyer, S. Park, C. W. Bielawski and R. S. Ruoff, The chemistry of graphene oxide, *Chem. Soc. Rev.*, 2010, **39**, 228–240, DOI: 10.1039/B917103G.
12 Z. Liu, J. T. Robinson, X. M. Sun and H. J. Dai, PEGylated nanographene oxide for delivery of water-insoluble cancer drugs, *J. Am. Chem. Soc.*, 2008, **130**, 10876–10877, DOI: 10.1021/ja803688x.
13 D. Li, M. B. Muller, S. Gilje, R. B. Kaner and G. G. Wallace, Processable aqueous dispersions of graphene nanosheets, *Nat. Nanotechnol.*, 2008, **3**, 101–105.https://www.nature.com/articles/nnano.2007.451.
14 Z. Bo, X. Guo, X. Wei, H. Yang, J. Yan and K. Cen, Density functional theory calculations of NO_2 and H_2S adsorption on group-10 transition-metal (Ni, Pd, Pt) decorated graphene, *Physica E, Low Dimens. Syst. Nanostruct.*, 2019, **109**, 156–163, DOI: 10.1016/j.physe.2019.01.012.
15 S. S. Varghese, *et al.*, Recent advances in graphene-based gas sensors, *Sens. Actuator B-Chem.*, 2015, **218**, 160–183, DOI: 10.1016/j.snb.2015.04.062, https://www.infona.pl/resource/bwmeta1.element.elsevier-023b41d7-0b6c-3b6a-bbda-ba8bb511629a.
16 G. Giovannetti, *et al.*, Doping graphene with metal contacts, *Phys. Rev. Lett.*, 2008, **101**, 026803, DOI: 10.1103/PhysRevLett.101.026803,https://pubmed.ncbi.nlm.nih.gov/18764212/.
17 A. S. Rad, Al-doped graphene as a new nanostructure adsorbent for halomethane compounds: DFT calculations, *Surf. Sci.*, 2016, **645**, 6–12, DOI: 10.1016/j.susc.2015.10.036, https://www.sciencedirect.com/science/article/pii/S0039602815003404.
18 H. Zhang, *et al.*, DFT calculations on the sorption of formaldehyde and other harmful gases on pure, Ti-doped, or N-doped graphene sheets, *Appl. Surf. Sci.*, 2013, **283**, 559–565, DOI: 10.1016/j.apsusc.2013.06.145, [Online] Available: https://www.sciencedirect.com/science/article/pii/S0169433213012580.
19 M. Baraket, *et al.*, Aminated graphene for DNA attachment produced via plasma functionalization, *Appl. Phys. Lett.*, 2012, **100**, 233123, DOI: 10.1063/1.4711771.
20 G. Shim, M. Kim, J. Y. Park and Y. Oh, Graphene-based nanosheets for delivery of chemotherapeutics and biological drugs, *Adv. Drug Delivery Rev.*, 2016, **105**(Part B), 205–227, DOI: 10.1016/j.addr.2016.04.004.
21 M. Vatanparast and Z. Shariatinia, AlN and AlP doped graphene quantum dots as novel drug delivery systems for 5-fluorouracil, *J. Fluorine Chem.*, 2018, **211**, 81–93, DOI: 10.1016/j.jfluchem.2018.04.003, https://www.sciencedirect.com/science/article/pii/S0022113917305092.
22 A. C. Rossi-Fernandez, *et al.*, Theoretical study of glycine adsorption on graphene oxide, *J. Mol. Model.*, 2020, **26**, 33, DOI: 10.1007/s00894-020-4297-8.
23 S. J. Rodriguez, L. Makinistian and E. Albanesi, Transport properties of graphene upon amino-acid adsorption, *J. Comput. Electron.*, 2017, **16**, 127–132, DOI: 10.1007/s10825-016-0943-x.
24 R. Zhiani, Adsorption of amino acids on graphene and BN nanosheets: a DFT-D3 study, *Appl. Surf. Sci.*, 2017, **409**, 35–44, DOI: 10.1016/j.apsusc.2017.02.243.
25 B. Saha and P. Bhattacharyya, Adsorption of amino acids on B- and/or N-doped graphene: a DFT study, *Comput. Theor. Chem.*, 2016, **1086**, 45–51, DOI: 10.1016/

j.comptc.2016.04.017, https://www.sciencedirect.com/science/article/pii/S2210271X16301426.
26 S. Narayan, P. K. Mishra and A. K. Singh, Dopant- and functional group-dependent modulation of electronic structure and adsorption behavior in graphene quantum dots: a DFT study, *RSC Adv.*, 2023, **13**, 28741–28752.
27 J. Feng, H. Dong, B. Pang, F. Shao, C. Zhang and L. Yu, Effects of heteroatom doping on the electronic structure and surface reactivity of graphene quantum dots: a density functional theory investigation, *Phys. Chem. Chem. Phys.*, 2018, **20**, 15244–15252.
28 M. A. Al-Amin, R. Islam and M. M. Rahman, First-principles insights into heteroatom-doped graphene quantum dots: stability, charge redistribution and adsorption characteristics, *RSC Adv.*, 2024, **14**, 11235–11247.
29 W. Qin, *et al.*, DFT and MD simulations of biomolecule adsorption on graphene, *Biomaterials*, 2010, **31**(5), 1007–1016, DOI: 10.1016/j.biomaterials.2009.10.013, https://www.sciencedirect.com/science/article/pii/S0142961209010886.
30 H. Vovusha, S. Sanyal and B. Sanyal, Interaction of nucleobases and aromatic amino acids with graphene oxide, *J. Phys. Chem. Lett.*, 2013, **4**, 3710–3718, DOI: 10.1021/jz401929h.
31 A. Ayatollahi, *et al.*, Adsorption characteristics of amino acids on graphene and germanene, *Physica E*, 2021, **127**, 114498, DOI: 10.1016/j.physe.2020.114498.
32 C. Rajesh, C. Majumder, H. Mizuseki and Y. Kawazoe, Interaction of aromatic amino acids with graphene and carbon nanotubes, *J. Chem. Phys.*, 2009, **130**(12), 124211, DOI: 10.1063/1.3079096.
33 R. Dennington, T. A. Keith, and J. M. Millam, *GaussView, Version 6*, Semichem Inc., 2016. https://gaussian.com/gaussview6.
34 M. J. Frisch et al., *Gaussian 16, Revision C.01*, Gaussian Inc., 2016, https://gaussian.com.
35 W. Kohn and L. J. Sham, Self-consistent equations including exchange and correlation effects, *Phys. Rev.*, 1965, **140**(A1133), DOI: 10.1103/PhysRev.140.A1133.
36 Y. Zhao and D. G. Truhlar, The M06 suite of density functionals for main group thermochemistry, thermochemical kinetics, noncovalent interactions, excited states and transition elements, *Theor. Chem. Acc.*, 2008, **120**, 215–241.
37 Y. Zhao and D. G. Truhlar, Density functionals with broad applicability in chemistry, *Acc. Chem. Res.*, 2008, **41**, 157–167.
38 W. J. Hehre, R. Ditchfield and J. A. Pople, Further extensions of Gaussian-type basis sets, *J. Chem. Phys.*, 1972, **56**, 2257–2261, DOI: 10.1063/1.1677527.
39 J. Řezáč and P. Hobza, Benchmark calculations of interaction energies in noncovalent complexes and assessment of DFT methods, *J. Chem. Theory Comput.*, 2013, **9**, 2151–2155.
40 S. Grimme, Do special noncovalent interaction functionals really improve the description of dispersion interactions?, *Angew. Chem., Int. Ed.*, 2008, **47**, 3430–3434.
41 K. Lee, É. D. Murray, L. Kong, B. I. Lundqvist and D. C. Langreth, Higher-accuracy van der Waals density functional, *Phys. Rev. B*, 2010, **82**, 081101.
42 C. H. Suresh and S. R. Gadre, Electrostatic and polarization contributions to molecular binding, *J. Phys. Chem. A*, 2007, **111**, 710–714.
43 R. M. Parrish and C. D. Sherrill, Quantum-mechanical evaluation of noncovalent π interactions, *J. Am. Chem. Soc.*, 2014, **136**, 17386–17389.
44 J. P. Merrick, D. Moran and L. Radom, An evaluation of harmonic vibrational frequency scale factors, *J. Phys. Chem. A*, 2007, **111**, 11683–11700.
45 M. L. Laury, M. J. Carlson and A. K. Wilson, Vibrational frequency scale factors for density functional theory, *J. Comput. Chem.*, 2012, **33**, 2380–2387.
46 A. Tavassoli Larijani, S. Farahani and M. Sedighipoor, Glycine–graphene interactions: a DFT study, *Phys. Chem. Chem. Phys.*, 2017, **19**, 14377–14388, DOI: 10.1039/C6CP06672K.
47 M. Ersan, E. Aktürk and S. Ciraci, Amino acid interaction with graphene and functionalized graphene, *J. Mol. Graphics Modell.*, 2020, **101**, 107722, DOI: 10.1016/j.jmgm.2020.107722, https://pubmed.ncbi.nlm.nih.gov/33098474/.
48 İ. Ersan, E. Aktürk and S. Ciraci, Glycine self-assembled on graphene enhances solar absorbance, *Carbon*, 2019, **146**, 390–399, DOI: 10.1016/j.carbon.2019.01.020.
49 S. F. Boys and F. Bernardi, Calculation of small molecular interactions by differences of separate total energies, *Mol. Phys.*, 1970, **19**, 553–566, DOI: 10.1080/00268977000101561.
50 M. F. Khan, J. Yu, Y. Park and S. H. Kim, Theoretical Study of Glycine Adsorption on Graphene Oxide, *J. Mol. Model.*, 2019, **25**, 28, DOI: 10.1007/s00894-018-3905-7.